Association of Fault Terminations With Fluid Flow in the Salt Wells Geothermal Field, Nevada, USA

Nicholas H. Hinz[1], James E. Faulds[1], and Mark F. Coolbaugh[2]

[1]Nevada Bureau of Mines and Geology, University of Nevada, Reno, USA
[2]Great Basin Center for Geothermal Energy, University of Nevada, Reno, USA

Keywords

Great Basin, Basin and Range, accommodation zone, fault termination, fault step-over, fault intersection, thermal anomaly, production wells, surface manifestations, alteration

ABSTRACT

The Salt Wells geothermal system is situated in a compound structural setting involving the termination of a major normal fault zone, a synclinal accommodation zone, and two prominent stepovers. The thermal anomaly, 12-km long, is principally coincident with a series of horsetail splays of the southward terminating Rainbow Mountain fault zone (RMFZ). Episodic dextral shear accommodated along north- to north-northeast-striking normal faults of the RMFZ further enhances permeability in this system. Surface manifestations at Salt Wells include hot springs, patches of warm ground, evaporate mineral deposits, silicified sediments and bedrock, opal sinter, and argillic alteration. Lateral heterogeneities of the thermal anomaly and the distribution of surface manifestations are spatially associated with terminating horsetail splays oriented perpendicular to the least principle stress. These clusters of fault splays probably correspond to critically stressed rupture arrest regions along the RMFZ, as reflected in the distribution of Quaternary fault scarps. The 14 MWe-capacity power plant produces from five production wells at depths of 60 to 150 meters and temperatures of 135 to 140°C in the southern quarter of the thermal anomaly. The production area corresponds to the hottest part of the system as defined by temperature gradient holes, lying within the southernmost splays of the southward terminating RMFZ. Maximum bottom-hole temperatures from a 2.5 km-deep well, abundant near-surface silica deposition, and fluid geothermometry from several springs and wells collectively indicate ~180 to 190°C reservoir temperatures and the potential for additional power production capacity from a deeper reservoir.

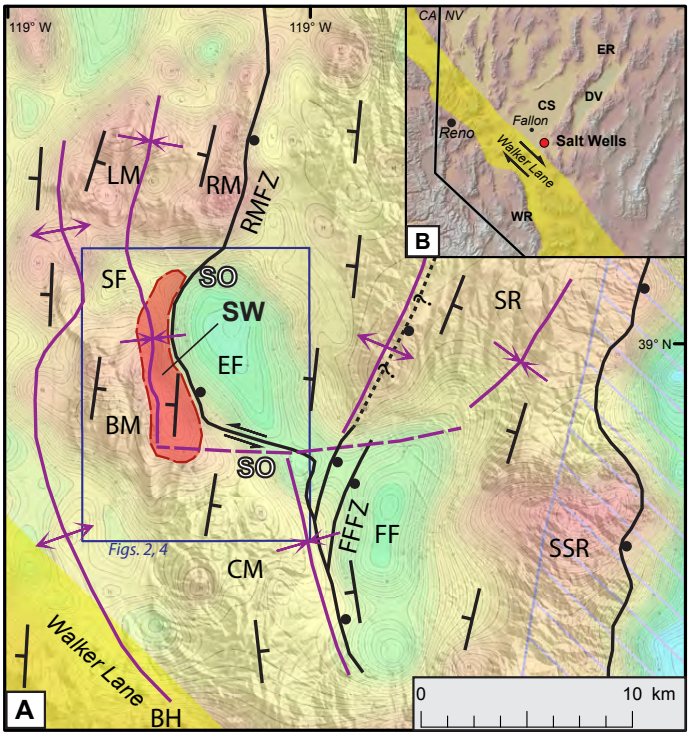

Figure 1. (**A**) Salt Wells area map with color coded first derivative CBA gravity model draped over shaded relief; gravity lows are depicted as green and gravity maximums depicted as pink (new gravity modeling, Faulds et al., 2014). The Salt Wells thermal anomaly is depicted by the semi-transparent pink-orange polygon (Edmiston and Benoit, 1984). Accommodation zone fold axes shown in solid purple lines and a single transverse-to structure accommodation zone is shown as a dashed purple line. Major faults are shown as solid black lines with balls on downthrown sides. Averaged strike and dip direction depicted with unannotated strike and dip symbols (Page, 1965; Bell et al., 2010; Bell and House, 2010; Hinz et al., 2011, unpublished mapping). BM, Bunejug Mountains; BH, Barnett Hills; CM, Cocoon Mountains; DV, Dixie Valley; EF, Eightmile Flat; FF, Fourmile Flat; FFFZ, Fourmile Flat fault zone; LM, Lahontan Mountains; RM, Rainbow Mountain; RMFZ, Rainbow Mountain fault zone; SF, Star Flat; SSR, Sand Springs Range; SR, Stillwater Range. (**B**) Regional location map of Salt Wells relative to the Walker Lane, Fallon, and Reno; CS, Carson Sink; ER, East Range; WR, Wassuk Range. Major fault stepovers in the RMFZ labeled SO.

Introduction

The Salt Wells geothermal field occupies the west margin of the Eightmile Flat basin ~25 km southeast of Fallon, Nevada (Fig. 1). Anadarko Petroleum Corporation, Hunt Oil Company, and the USGS first conducted geothermal exploration in the area in the 1970s and 1980s with geophysical surveys, and the drilling of temperature gradient holes and test wells. Temperature gradient drilling defined a 12 km-long thermal anomaly elongate north-south (Fig. 1; Edmiston and Benoit, 1984). A 2591 m-deep exploration well drilled in 1978 recorded a maximum bottom-hole temperature of 181°C. Amp Resources, LLC, expanded efforts to develop this resource in the early 2000s before being acquired by Enel Green Power North America, Inc. in 2007. Subsequently, Enel developed a 14 MWe capacity power plant that was brought online in 2009 with five production wells (Nevada Division of Minerals data). In 2013 a new production well was added at the south end of the production field, whereas the northernmost production well was disconnected, leaving the power plant to continue operation with five production wells and effectively nudging the overall production well-field footprint farther south by ~500 m.

Initial research on the controls of the Salt Wells geothermal system identified a compound structural setting, including both the southward termination of the RMFZ and a synclinal accommodation zone between predominantly west-dipping faults in the Bunejug Mountains and east-dipping faults in the Eightmile flat basin (Faulds et al., 2006). The Salt Wells geothermal area is associated with extensive inactive, and less abundant active surface manifestations (Coolbaugh et al., 2004; 2006), which along with thermal and geophysical data help highlight key spatial and temporal constraints on geothermal activity. This paper presents new details on the structural controls of the Salt Wells geothermal system inferred from ongoing detailed geologic mapping and structural analyses of faults, folds, and veins (e.g., Hinz et al., 2011).

Tectonic Setting

The Salt Wells geothermal area resides in the northern Basin and Range extensional province and immediately northeast of the Walker Lane. The Walker Lane is a belt of concentrated dextral shear along a distributed set of strike-slip, normal, and normal-oblique-slip faults in the western part of the Basin and Range that collectively accommodate ~20-25% of the relative Pacific-North American Plate Motion (e.g., Faulds and Henry, 2008; Fig. 1B). Regional studies in west-central Nevada constrain the onset of Basin and Range extension to ~17-15 Ma in the East Range (Fig. 1B; Fosdick and Colgan, 2008) and ~15-12 Ma in the Wassuk Range area (Stockli et al., 2002). A 14 Ma north-striking basaltic dike swarm exposed in both the Bunejug Mountains and in Rainbow Mountain may correspond to the onset of extension in the Basin and Range in the Salt Wells area (Bell et al., 2010; Hinz et al., 2011). Miocene lacustrine sediments resting non-conformably on 12 Ma lavas in the Lahontan Mountains probably represent initial local sedimentary accumulation in extensional basins (Bell et al., 2010). Dextral shear began ~9-10 Ma in the north-central Walker Lane west of Salt Wells (Faulds and Henry, 2008); however despite relatively close proximity (Fig. 1), the tectonic fabric of the Salt Wells region is dominated by extensional faults and folds rather than dextral shear or wrench faulting. This contrasts greatly with fault patterns mapped at the Lee-Allen geothermal area, 15 km southwest of Salt Wells (Hinz et al., 2008; 2010).

Stratigraphic Framework

In the Salt Wells area, Neogene volcanic and sedimentary strata rest unconformably on Mesozoic basement. Mesozoic basement is not exposed within the Salt Wells geothermal area, and only one well, 14-36, intersects Mesozoic granite within this area at 670 m-depth. Another two wells, FOH-1 and FOH-3, ~15 km west-northwest of Salt Wells in the Carson Sink, intersect Mesozoic granitic, volcanic, and sedimentary units. Based on basement exposures within a 15 to 25 km radius of Salt Wells (Fig. 1A) in the southeastern Stillwater Range (John and Silberling, 1994) the Sand Springs Range (Page, 1965; Satterfield, 2002), the Barnett Hills (Stewart and Carlson, 1978), and at the Lee-Allen geothermal area (Hinz et al., 2010), the Mesozoic basement associated with the Salt Wells geothermal area is probably dominantly granitic with possible metasedimentary and metavolcanic units.

The Neogene volcanic and sedimentary rocks range in thickness from 0.75 km in the Bunejug Mountains to ~2.5 km the Eightmile Flat basin (Hinz et al., 2011; well 14-36; unpublished gravity modeling in Faulds et al., 2014). The Miocene strata in the Bunejug Mountains, Cocoon Mountains, and Rainbow Mountains consist of >16-12 Ma mafic lavas locally interbedded with minor tuffs, sediments, and felsic lavas (Fig. 1A; Bell et al., 2010; Hinz et al., 2011). A >1 km-thick section of fine-grained late Miocene or Pliocene to Holocene lacustrine sediments cover the Miocene volcanic sequences in the Eightmile Flat and Fourmile Flat basins. The footprint of the Salt Wells geothermal area is dominated by latest Pleistocene lacustrine and Holocene alluvial and eolian deposits, with Miocene bedrock only exposed along the higher relief areas and along incised alluvial channels or erosional Late Pleistocene pluvial shorelines (Figs. 1A, 2; Hinz et al., 2011).

Structural Framework

The Salt Wells area is dominated by two prominent west-tilted half-grabens (EF and FF, Fig. 1A), each ~2.5 km deep, bounded by east-dipping normal faults along their western margins. The Fourmile Flat basin is bound by the ~15 km-long Fourmile Flat fault zone (FFFZ) and the Eightmile Flat Basin is bound by the southern part of the ~25 km-long RMFZ. A prominent west-northwest-striking dextral fault links the FFFZ and the RMFZ across a 6 km-wide stepover at the north end of the Cocoon Mountains. As the RMFZ rounds the southern tip of Rainbow Mountain, it makes a 2 km-wide right step coincident with the northwest corner of Eightmile Flat. South of this right step, the RMFZ bifurcates into multiple horsetail splays in the footwall side of the primary fault trace along nearly the entire western margin of Eightmile Flat, and extending south into Simpson Pass (Fig. 2). In addition to the two primary fault zones, the FFFZ and RMFZ, numerous north-northwest- to north-northeast-striking normal faults with 10s to 100s of meters of stratigraphic offset cut the Mio-Pliocene strata in the ranges surrounding Eightmile Flat and Fourmile Flat. Together, these moderate-offset normal faults and the large-offset fault zones (RMFZ and FFFZ) and comprise multiple dip domains through the area, yielding three synclinal

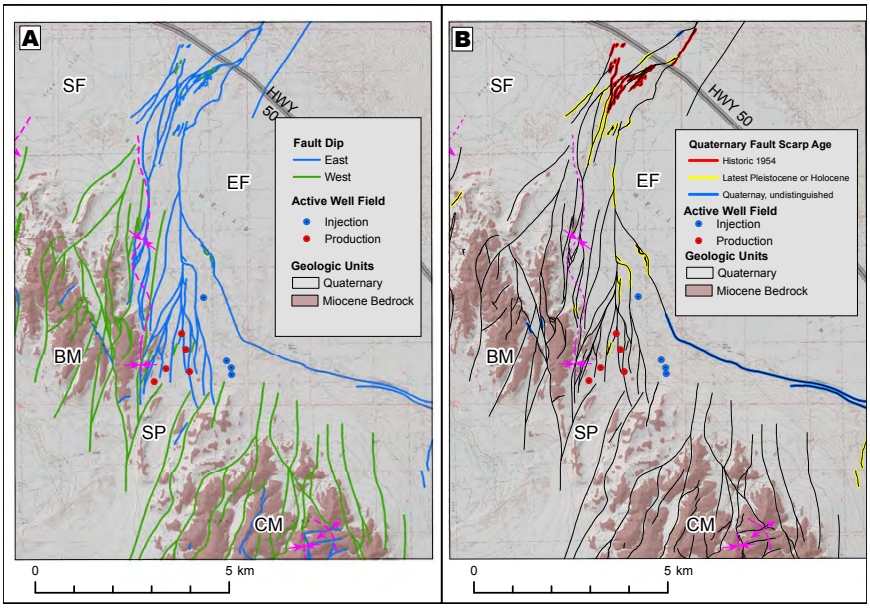

Figure 2. Simplified geologic map showing the distribution of Miocene bedrock, Quaternary surficial units, faults, and folds relative to the active production and injection wells (Hinz et al., 2011, unpublished mapping). For simplicity, all faults are shown as solid lines including concealed segments. Fault dip directions are color coded by dip direction in **(A)** and by age of most recent displacement in **(B)**. Places referenced in text: BM, Bunejug Mountains; CM, Cocoon Mountains, EMF, Eightmile Flat; SF, Star Flat; SP, Simpson Pass.

accommodation zones, two anticlinal accommodation zones, and one transverse accommodation zone.

The RMFZ and FFFZ are both associated with Quaternary fault scarps (Figs. 1, 2). Major sections of both the RMFZ and the FFFZ ruptured in two closely spaced, but separate events, on July 6, 1954. Paleoseismic studies of these two fault zones have documented two prehistoric events on the RMFZ, one being latest Pleistocene and one being Holocene, and two prehistoric events on the FFFZ, both of Holocene age (Caskey et al., 2004). The historic 1954 ruptures extend over much of the RMFZ to the north, and terminate southward near the northern end of the Salt Wells geothermal area. Of the faults mapped through the geothermal area, relatively few segments are associated with Quaternary fault scarps, and most of these are associated with east-dipping strands of the RMFZ and the dextral transfer fault connecting the RMFZ to the FFFZ.

Examination of fault surfaces exposed in Miocene bedrock yielded slip azimuths of two primary sets. One set indicates approximate east-west to west-northwest—east-southeast extension and the other indicates north-south oriented dextral-oblique to pure dextral motion on pre-existing normal faults. Although the RMFZ is dominantly normal-slip, data from fault surfaces collected in the bedrock and from the 1954 faults indicate episodic dextral slip along north-northwest- to northeast-striking normal fault segments.

Silica veins were observed in outcrops of Miocene bedrock and silicified sediments. Silica veins in the bedrock were only observed near silicified sediment and in areas of hydrothermally altered bedrock, generally within the modern-day thermal anomaly. The dominant orientation of the veins are north to north-northeast striking with subvertical dips and imply a least principle stress ($\sigma 3$) orientation of east-west to west-northwest—east-southeast. These results are nearly identical to that derived from stress inversion of fault slip data and analysis of borehole breakouts and tensile fractures in well FOH-3 in the southeastern part of the Carson Sink, N83°W (Blake and Davatzes, 2012).

Alteration and Silicification

Outcrops of argillically altered bedrock are distributed throughout the southern two thirds of the geothermal area, and bedrock is simply not

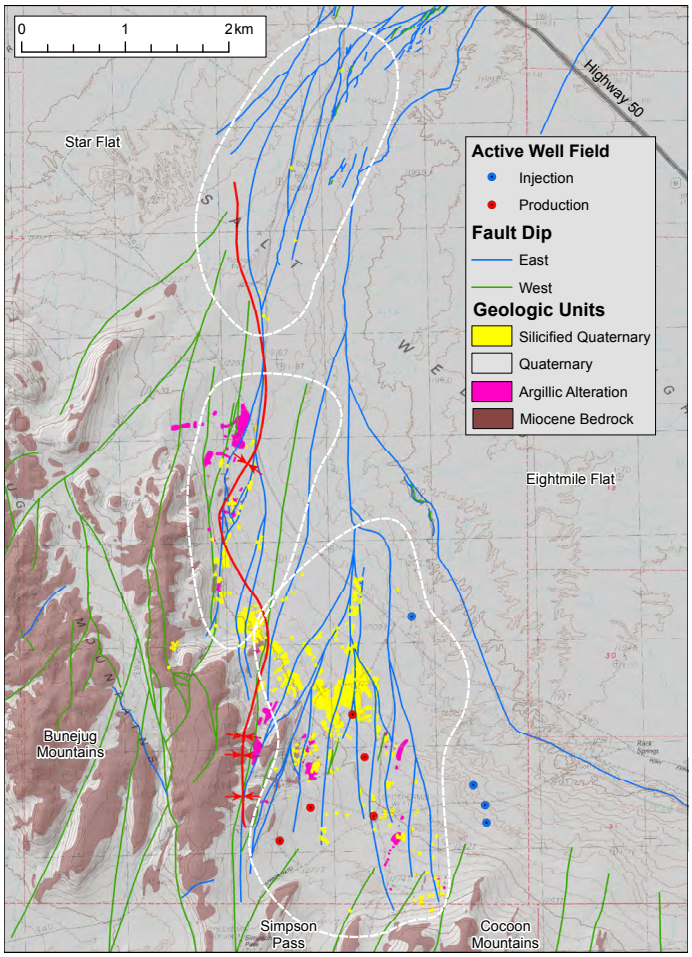

Figure 3. Detailed distribution of silicified Quaternary sediments (yellow) and argillic altered bedrock (magenta) displayed on the same base figure as Figure 2A with simplified geologic units, faults illustrated according to dip direction, and folds (modified from Coolbaugh et al. (2004), Hinz et al., (2011); and Hinz, unpublished mapping). The areas of argillic alteration includes lumped distribution of high, moderate, and low intensity alteration, with the degree of alteration of most outcrops in the low to moderate range. Dashed white lines correspond to locally elevated temperature data within the broad Salt Wells geothermal anomaly as defined in Figure 4. Places referenced in text: BM, Bunejug Mountains; CM, Cocoon Mountains, EMF, Eightmile Flat; SF, Star Flat; SP, Simpson Pass.

exposed in the northern third of the area (Fig. 3). About half of the argillically altered bedrock has also been silicified and locally contains abundant silica veins. In most places where silica veins were noted in bedrock in contact with Late Pleistocene or Holocene sediments, the overlying sediments were not silicified, indicating that both the argillic alteration and subsequent silicification of the bedrock occurred prior to deposition of the Late Quaternary sediments.

Outcrops of silicified Quaternary sediments span nearly the entire geothermal area, with the most extensive outcrops in the southern two thirds (Fig. 3). These include silicified eolian and alluvial deposits of the Wyemaha Alloformation (150 to 35 ka), lacustrine deposits of the Sehoo Alloformation (35 to 11 ka), and Holocene alluvial and eolian deposits (ages of Wyemaha and Sehoo from Bell et al., 2010; Bell and House, 2010). In areas where the Wyemaha sediments are silicified, the overlying or adjacent Sehoo deposits are also consistently silicified, probably placing the age of silicification post-Wyemaha. Holocene alluvial fan and eolian deposits that onlap the silicified Sehoo deposits are only locally silicified. Together, these relationships indicate surface discharge of silica-rich fluids in both the Late Pleistocene and Holocene time in areas where spring activity has not been observed historically. Current-day silicification has been observed in the root zone of marsh grasses adjacent to hot springs along the western margin of Eight-Mile Flat (Coolbaugh et al., 2006). The fact that shallow-level silicification is an ongoing process associated with the active Salt Wells geothermal system is supported by high silica contents of thermal fluids (>200 mg/l SiO2) and high fluid quartz geothermometry (~190°C). The location of silicification appears to have shifted eastward in step with the eastward migration of thermal springs as the water table dropped during the drying of Lake Lahontan.

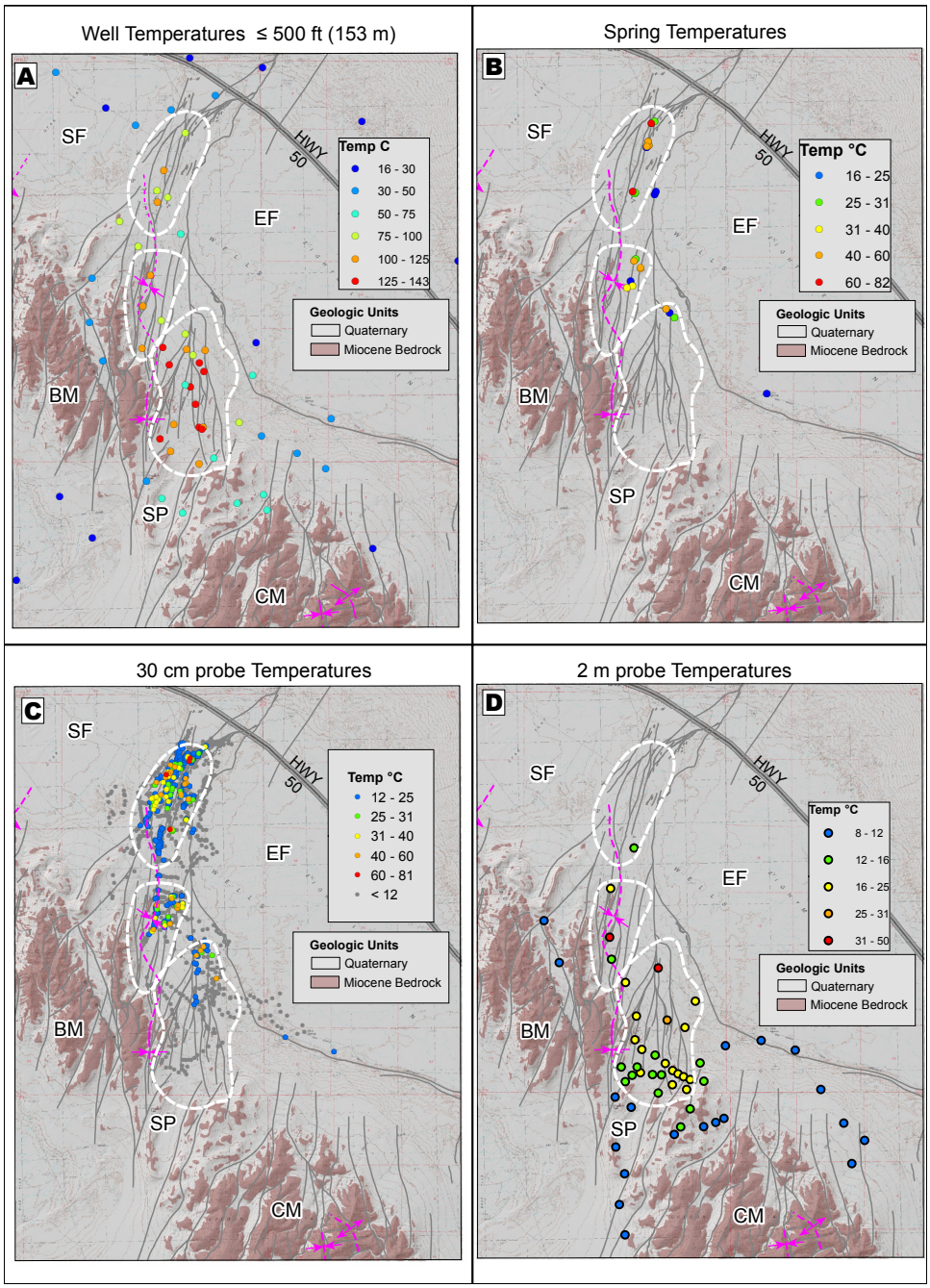

Figure 4. Thermal data measurements for the Salt Wells geothermal area including, **(A)** 500 foot temperature gradient holes, **(B)** spring temperatures (Coolbaugh et al., 2006), **(C)** 30 cm probe temperatures (Coolbaugh et al., 2006), and **(D)** two meter probe temperatures (Skord, 2012). Dashed white lines correspond to locally elevated temperature data within the broad Salt Wells geothermal anomaly as illustrated by collective interpretation of these data sets. Basemap is from Figure 2. Places referenced in text: BM, Bunejug Mountains; CM, Cocoon Mountains, EMF, Eightmile Flat; SF, Star Flat; SP, Simpson Pass.

Thermal Data

Multiple data sets define the thermal anomaly of Salt Wells and include temperature gradient holes, wells, springs, two meter temperature probes, 30 cm temperature probes, and fluid geothermometry calculations (Fig. 4). Each thermal data set inherently provides a slightly different perspective on the anatomy of this geothermal system and is also available with differing spatial coverage. Assessed both individually and in sum, these data sets provide key insights into discrete controls on fluid flow.

Temperature Gradient Holes and Wells

Of all the thermal data sets, only the shallow temperature gradient holes and wells, ≤ 500 feet deep (~153 m) cover the entire geothermal area and define the 12-km long thermal anomaly (Figs. 1A, 4A; Edmiston and Benoit, 1984). The highest temperature

gradient holes (125 to 143°C) are in the southern third of the geothermal area and are generally coincident with the five active production wells that produce from depths of 60 to 150 meters and temperatures of 135-140°C (Nevada Division of Minerals data). In addition to the temperature gradient holes and active production wells, additional shallow to moderate depth production and injection wells ranging from 150 to 500 m deep have been drilled in the southern half of the geothermal area, and generally corroborate the anomaly constrained by the temperature gradient holes. In 1978, one deep exploration well was drilled at Salt Wells in the middle of what is now the modern production well field and recorded a maximum bottom-hole temperature of 181°C at 2591 m. This peak measured temperature is consistent with quartz and Mg-corrected Na-K-Ca geothermometry calculated from springs and wells that range from 162 to 214°C, averaging 185°C (Coolbaugh et al., 2006).

Hot Springs

Hot springs and seeps have been recognized at Salt Wells since the late 1800s (Russell, 1885; Peale, 1886; Stearns et al., 1937; Coolbaugh et al., 2006). Active springs are restricted to the eastern margin and lowest elevation areas of the geothermal area (Fig. 4B). Most of these springs are aligned along primary splays of the RMFZ along the west and northwest margins of Eightmile Flat. The single primary spring in the southeast part of the area is cold and is also the only spring located in the hanging wall of the primary trace of the RMFZ. Borate deposits were identified and mined during the 1870s in the northern part of the Salt Wells geothermal area, and these deposits are interpreted to indicate relatively prolonged hot spring activity (Papke, 1976; Kratt et al., 2006).

30 cm Temperature Probe

Nearly the entire geothermal field was covered by approximately a thousand 30-cm-deep temperature probe measurements, providing greater overall point density than any other thermal data set (Fig. 4C; Coolbaugh et al., 2006). This technique is strongly influenced by the presence/absence of a shallow, near-surface water table. For example, in the southern part of the geothermal area, numerous 30 cm probe measurements record cool temperatures adjacent to warm 2 m probe measurements (Fig. 4C, D). However, this data set clearly defined multiple thermal anomalies that coincide tightly with several of the mapped fault traces in the northern half of the geothermal field.

2 m Temperature Probe

Two meter data is restricted to the southern two thirds of the geothermal field and illustrates two potentially separate hot spots within the area (Fig. 4D; Skord et al., 2011; Skord, 2012). One area generally corresponds to the production well field area and the other area to a prominent cluster of fault intersections in the central portion of the geothermal area, adjacent to intensely argillically altered outcrops of bedrock (Fig. 3). The highest 2m temperatures associated with the production well field area are located at the north end and may signal shallow outflow from this area in a north-northeast direction along the structural grain of the fault strands.

Heterogeneity in each of these data sets shows evidence for multiple smaller hot-spot anomalies within the upper 500 feet of this geothermal system. Taking into account the results of all four thermal data sets, three separate shallow thermal anomalies were distinguished (Fig. 4). These relative hot spots are also generally coincident with soil gas anomalies identified by Skord (2012) and the southernmost area coincides with an electromagnetic anomaly designed to identify reservoir fluids (Montgomery et al., 2005).

Discussion

The Salt Wells geothermal area resides in an area of pronounced structural complexity including abundant splays of the southward terminating RMFZ and a synclinal accommodation zone involving overlapping east- and west-dipping normal faults. Furthermore, all of these features are bracketed between two stepovers. Each of these major structural environments is typically associated with relatively high density of faults, fractures, and intersections of faults and fractures, which collectively enhances permeability that facilitates convection of geothermal fluids (e.g., Faulds et al., 2006; 2011). The importance of compound or hybrid structural settings, involving two-or-more structural settings, has been highlighted for actively producing systems in the Basin and Range (Faulds et al, 2013). Adding to the compound nature of the structures related to this system, episodic dextral slip along north-striking fault segments documented along the 1954 historic scarps and on older fault surfaces may further enhance permeability at right steps and along down-dip corrugations (e.g., Micklethwaite, 2009).

Of all the structural influences on geothermal activity at Salt Wells, the fault termination splays correlate most closely with the lateral extent and heterogeneities of the thermal anomaly. The entire thermal anomaly resides between two fault stepovers, but the core of the thermal anomaly does not correlate closely with either stepover. The synclinal accommodation zone parallels much of the thermal anomaly, however the fold axis runs ~ 1km west of the highest temperatures, and the thermal anomaly and fold axis completely diverge in the northern part of the area. Arcuate in shape, the overall thermal anomaly is bound on the east by the primary trace of the RMFZ as it curves around the west side of Eightmile Flat, residing entirely in the footwall of the primary strand of the RMFZ. This footwall region is cut by numerous fault splays that strike from northwest to northeast. Each of the primary hot spots depicted in Figure 4 is associated with a local horsetail cluster of faults with primarily east-northeast-strikes, which are perpendicular to the inferred west-northwest/east-southeast extension direction. The southernmost hot spot, which is associated with the final group of terminating splays of the RMFZ, is also associated with the active production well field.

Most of the outcrops of silicified sediments sit at the south end/southwest side of the geothermal area, at generally higher elevation than the active hot springs. The entire geothermal field was submerged by pluvial Lake Lahontan during the late Pleistocene Sehoo cycle. Field relationships indicate that most of the silicified sediments were probably silicified during Sehoo time, when the water table was higher. Higher temperature drill holes and/or greater volume of silicified sediments support robust upflow in the distal fault termination splays. The extent of active springs today may simply result from a lowering of the water table relative to the Late Pleistocene.

Fault tips are typically associated with complex damage zones (McGrath and Davison, 1995; Kim et al., 2004), and enhanced fluid flow in these regions has been well documented (Curewitz and Karson, 1997; Cox et al., 2001; Rowland and Sibson, 2004; Faulds et al., 2006, 2011). Terminations of major normal faults can also result in both along-strike and up or down-dip horsetail splays (e.g., Granier, 1985). Horsetail splay networks form in rupture arrest regions that have been associated with elevated permeability (Sibson, 1987; Micklethwaite and Cox, 2004) and have been specifically recognized as important fluid flow conduits for epithermal gold and porphyry copper deposits (e.g., Perry, 1950; Granier, 1985). All three hot spots are located south of the 1954 surface ruptures, and the southernmost hot spot that contains the production well field is only associated with one potential Quaternary scarp. The general absence of Quaternary fault scarps within the production well field corresponds with arrest of fault slip in this region of abundant fault splays. Consistent with previous studies in the Great Basin (Bell and Ramelli, 2007; Faulds et al., 2012), whereby most of the higher temperature systems are associated with Holocene-active fault zones, the best location for the production well field may fall along segments where Quaternary fault scarps are locally sparse or absent and the fault zone is critically stressed.

Acknowledgments

This work was supported through multiple sources of funding including the U.S. Geological Survey STATEMAP Program (Agreement No. G10AC00220) awarded to Hinz and Faulds, the Great Basin Center for Geothermal Research at the University of Nevada, Reno and Department of Energy (Agreement No. DE-FG36-02ID14311) awarded to Faulds, and an American Recovery and Reinvestment Act grant from the Department of Energy (Agreement No. EE0002748) awarded to Faulds. We thank Danny Lazzareschi on behalf of Enel Green Power North America, Inc. for providing access to temperature gradient hole data used to develop Figure 4A. Interpretations of Quaternary geology presented in this paper have benefited greatly from numerous discussions with John Bell. We also thank Joe Moore for providing a thoughtful and thorough review of this paper.

References Cited

Bell, J.W. and House, P.K., 2010, Geologic Map of the Grimes Point Quadrangle, Churchill County, Nevada: Nevada Bureau of Mines and Geology Map 173, 1:24,000 scale, 1 sheet, 24 p.

Bell, J.W., and Ramelli, A.R., 2007, Active faults and neotectonics at geothermal sites in the western Basin and Range: Preliminary results: Geothermal Resources Council Transactions, v. 31, p. 375-378.

Bell, J.W., Caskey, S.J., and House, P.K., 2010, Geologic Map of the Lahontan Mountains Quadrangle, Churchill County, Nevada: Nevada Bureau of Mines and Geology Map 168, 1:24,000 scale, 1 sheet.

Blake, K., and Davatzes, N.C., 2012, Borehole image log and statistical analysis of FOH-3D, Fallon Naval Air Station, NV: Proceedings, Thirty-Seventh Workshop on Geothermal Reservoir Engineering, Stanford University, p. 1-14.

Caskey, S.J., Bell, J.W., Ramelli, A.R., and Wesnousky, S.G., 2004, Historical surface faulting and paleoseismicity in the area of the 1954 Rainbow Mountain-Stillwater earthquake sequence, central Nevada: Bulletin of the Seismological Society of America, v. 94, no. 4, p. 1255-1275.

Caskey, S.J., Wesnousky, S.G., Zhang, P., and Slemmons, D.B., 1996, Surface Faulting of the 1954 Fairview Peak (M_s7.2) and Dixie Valley (M_s6.8) Earthquakes, Central Nevada: Bulletin of the Seismological Society of America, v. 86, no. 3, p. 761-787.

Coolbaugh, M.F., Sladek, C., and Kratt, C., 2004, Digital mapping of structurally controlled geothermal features with GPS units and pocket computers: Geothermal Resources Council Transactions, v. 28, p. 321-325.

Coolbaugh, M.F., Sladek, C., Kratt, C., Shevenell, L., and Faulds, J.E., 2006, Surface indicators of geothermal activity at Salt Wells, Nevada, USA, including warm ground, borate deposits, and siliceous alteration: Geothermal Resources Council Transactions, v. 30, p. 399-405.

Cox, S.F., Braun, J., Knackstedt, M.A., 2001, Principles of structural control on permeability and fluid flow in hydrothermal systems: Reviews in Economic Geology, v. 14, p. 1–24.

Curewitz, D. and Karson, J.A., 1997, Structural settings of hydrothermal outflow: fracture permeability maintained by fault propagation and interaction: Journal of Volcanology and Geothermal Research, v. 79, p. 149-168.

Doser, D.I., 1986, Earthquake Processes in the Rainbow Mountain-Fairview Peak-Dixie Valley, Nevada, Region 1954-1959: Journal of Geophysical Research, v. 91, no. B12, p. 12,572-12,586.

Edmiston, R.C. and Benoit, W.R., 1984, Characteristics of basin and range geothermal systems with fluid temperatures of 150°C to 200°C: Geothermal Resources Council Transactions, v. 8, p. 417-424.

Faulds, J.E., and 8 others, 2014, Final Research Performance Report: Characterizing Structural Controls of EGS-Candidate and Conventional Geothermal Reservoirs in the Great Basin: Developing Successful Exploration Strategies in Extended Terranes: Final Report to the DOE EERE Geothermal Technologies Program, Agreement Number DE-EE0002748, 54 p.

Faulds, J.E., and Henry, C.D., 2008, Tectonic influences on the spatial and temporal evolution of the Walker Lane: An incipient transform fault along the evolving Pacific – North American plate boundary, in Spencer, J.E., and Titley, S.R., eds., Ores and orogenesis: Circum-Pacific tectonics, geologic evolution, and ore deposits: Arizona Geological Society Digest 22, p. 437-470.

Faulds, J.E., Coolbaugh, M.F., Vice, G.S., and Edwards, M.L., 2006, Characterizing structural controls of geothermal fields in the north-western Great Basin: A progress report: Geothermal Resources Council Transactions, v. 30, p. 69-75.

Faulds, J.E., Hinz, N.H., and Kreemer, C.W., 2012, Regional patterns of geothermal activity in the Great Basin Region, western USA: Correlation with strain rates: Geothermal Resources Council Transactions, v. 36, p. 897-902.

Faulds, J.E., Hinz, N.H., Coolbaugh, M.F., Cashman, P.H., Kratt, C., Dering, G., Edwards, J., Mayhew, B., and McLachlan, H., 2011, Assessment of favorable structural settings of geothermal systems in the Great Basin, Western USA: Geothermal Resources Council Transactions, v. 35, p. 777-784.

Faulds, J.E., Hinz, N.H., Dering, G.M., and Siler, D.L., 2013, The hybrid model – the most accommodating structural setting for geothermal power generation in the Great Basin, western USA: Geothermal Resources Council Transactions, v. 37, p. 3-10.

Fosdick, J.C., and Colgan, J.P., 2008, Miocene extension in the East Range, Nevada: A two-stage history of normal faulting in the northern Basin and Range: Geosphere, v. 120, no. 9/10, p. 1198-1213.

Granier, T., 1985, Origin, damping, and pattern of development of faults in granite: Tectonics, v. 4, no. 7, p. 721-737.

Hinz, N.H., Faulds, J.E. and Oppliger, G.L., 2008, Structural controls of Lee-Allen Hot Springs, southern Churchill County, western Nevada: A

small pull-apart in the dextral shear zone of the Walker Lane: Geothermal Resources Council Transactions, v. 32, p. 285-290.

Hinz, N.H., Faulds, J.E., and Bell, J.W., 2011, Preliminary geologic map of the Bunejug Mountains Quadrangle, Churchill County, Nevada: Nevada Bureau of Mines and Geology Open-File Report 11-9, 1 sheet, 1:24,000 scale.

Hinz, N.H., Faulds, J.E., and Oppliger, G. L., 2010, Preliminary geologic map of the Lee-Allen geothermal area, Churchill County, Nevada: Nevada Bureau of Mines and Geology Open-File Report 10-6, 1 sheet, 1:24,000 scale with 1:8,000 scale inset.

John, D.A., and Silberling, N.J., 1994, Geologic Map of the La Plata Canyon Quadrangle, Churchill County, Nevada: U.S. Geological Survey Geological Quadrangle Map 1710, 1 sheet, 1:24,000 scale, 8 p.

Kim, Y-S, Peacock, D.C.P., and Sanderson, D.J., 2004, Fault damage zones, Journal of Structural Geology, v. 26, p. 503-517.

Kratt, C., Coolbaugh, M., and Calvin, W., 2006, Remote detection of Quaternary borate deposits with ASTER satellite imagery as a geothermal exploration tool: Geothermal Resources Council Transactions, v. 30, p. 435-439.

McGrath, A.G., and Davison, I., 1995, Damage zone geometry around fault tips: Journal of Structural Geology, v. 17, no. 7, p. 1011-1024.

Micklethwaite, S., 2009, Mechanisms of faulting and permeability enhancement during epithermal mineralization: Cracow goldfield, Australia: Journal of Structural Geology, v. 31, p. 288-300.

Micklethwaite, S., and Cox, S.F., 2004, Fault-segment rupture, aftershock-zone fluid flow, and mineralization: Geology, v. 32, no. 9, p. 813-816.

Montgomery, J., Bowers, R.L., and Kofoed, V., 2005, Characterization of Geothermal Resources using New Geophysical Technology: Geothermal Resources Council Transaction, v. 29, p. 489-492.

Page, B.M., 1965, Preliminary geologic map of part of the Stillwater Range, Churchill County, Nevada: Nevada Bureau of Mines and Geology Map 28, 1 sheet, 1:125,000 scale.

Papke, K.G., 1976, Evaporites and brines in Nevada playas: Nevada Bureau of Mines and Geology Bulletin 87, 35 p.

Peale, A.C., 1886, Lists and analyses of the mineral springs of the United States: U.S. Geological Survey Bulletin 32, 235 p.

Perry, E.S., 1950, The Butte mining district: Billings Geological Society First Annual Field Conference, p. 66-71.

Rowland, J.V., and Sibson, R.H., 2004, Structural controls on hydrothermal flow in a segmented rift system, Taupo Volcanic Zone, New Zealand: Geofluids, v. 4, p. 259–283.

Russell, I.C., 1885, Geological history of Lake Lahontan, a Quaternary Lake of northwestern Nevada: United States Geological Survey Monograph M11, 288 p.

Satterfield, J.I., 2002, Geology map of the southern Sand Springs Range: Nevada Bureau of Mines and Geology Map 133, 16 pages, 1 sheet, scale 1:24,000.

Sibson, R.H., 1987, Earthquake rupturing as a mineralizing agent in hydrothermal systems: Geology, v. 15, p. 701–704.

Skord, J., 2012, Interpretation of upwelling zones and structural controls at Lee Allen and Salt Wells geothermal fields [M.S. thesis]: University of Nevada, Reno, 110 p.

Skord, J., Cashman, P.H., Coolbaugh, M., and Hinz, N.H., 2011, Mapping hydrothermal upwelling outflow and outflow zones, preliminary results from two-meter temperature data and geologic analysis at Lee Allen Springs and Salt Wells basin, Geothermal Resources Council Transactions, v. 35, p. 1017-1022.

Stearns, N.D., Stearns, H.T., and Waring, G.A., 1937, Thermal springs in the United States: U.S. Geological Survey Water Supply Paper 679-B, p. 59-206.

Stewart, J.H., and Carlson, J.E., 1978, Geologic Map of Nevada: United States Geological Survey MF-930, 1:500,000 scale, 1 sheet.

Stockli, D.F., Surpless, B.E., Dumitru, T.A., and Farley, K.A., 2002, Thermochronological constraints on the timing and magnitude of Miocene and Pliocene extension in the central Wassuk Range, western Nevada: Tectonics, v. 21, 4, 10.1029/2001TC001295.